Electronic properties, doping, and defects in chlorinated silicon nanocrystals

A. Carvalho*
Department of Physics, I3N, University of Aveiro, Campus Santiago, 3810-193 Aveiro, Portugal

S. Öberg and M. J. Rayson
Department of Engineering Sciences and Mathematics, Luleå University of Technology, Luleå S-97187, Sweden

P. R. Briddon
Electrical, Electronic and Computer Engineering, University of Newcastle upon Tyne, Newcastle upon Tyne NE1 7RU, United Kingdom
(Received 15 November 2011; published 9 July 2012)

Silicon nanocrystals with diameters between 1 and 3 nm and surfaces passivated by chlorine or a mixture of chlorine and hydrogen were modeled using density functional theory, and their properties compared with those of fully hydrogenated nanocrystals. It is found that fully and partially chlorinated nanocrystals are stable, and have higher electron affinity, higher ionization energy, and lower optical absorption energy threshold. As the hydrogenated silicon nanocrystals, chlorinated silicon nanocrystals doped with phosphorus or boron require a high activation energy to transfer an electron or hole, respectively, to undoped silicon nanocrystals. The electronic levels of surface dangling bonds are similar for both types of surface passivation, although in the chlorinated silicon nanocrystals some fall outside the narrower energy gap.

DOI: 10.1103/PhysRevB.86.045308 PACS number(s): 61.72.Bb, 61.80.Az, 71.55.Cn

I. INTRODUCTION

The manipulation of the silicon surface and its ability to interact with molecules and radicals is gaining importance in view of the use of silicon nanostructures in hybrid inorganic-organic colloids and other functional materials. With a large surface-to-volume ratio, free-standing silicon nanocrystals (NCs) are ideal to explore the surface functionality. They can be obtained by ultrasonic dispersion of porous silicon,[1] liquid phase synthesis by reduction of $SiCl_4$,[2] or plasma processes.[3–9] Nonthermal plasma synthesis is an efficient method for production of particles of monodisperse sizes and lists, among other advantages, suppressed particle coagulation and selective heating of particles through energetic surface reactions.[3] Additionally, it offers the possibility of dopant (P,B) incorporation during growth.[10–13]

Although silane is usually chosen as a precursor for plasma synthesis, $SiCl_4$ has also been suggested as a cheaper and safer alternative.[7,8] Nanocrystals grown from a $SiCl_4/H_2/Ar$ mixture are terminated with a mixture of chlorine and hydrogen, with variable fractions depending on the plasma composition and reactor pressure.[7,8]

The fraction of surface Cl on silicon nanocrystals grown by this or other methods can also be increased by Cl_2 plasma etching, treatment with a solution of PCl_5 on chlorobenzene, or with di-, tri-, and tetrachlorosilane gases, procedures already in use for industrial processing of silicon single crystal substrates.[14] This leads to the formation of mono-, di-, and trichloride terminations at low temperatures ($<400\,^{\circ}C$).[15] Monochloride is the most stable, remaining at higher temperature. The adsorption of chlorine and $SiCl_n$ on flat silicon surfaces has been extensively studied by theoretical methods.[16–22] The adsorption energy of Cl_2 on a reconstructed Si(100) surface was found to be 5.4 eV,[16] giving a Si-Cl bond energy of about 4 eV. On Si(111) surfaces, the Si-Cl bond energy is similar, the calculated values ranging between 3.5 and 4.2 eV.[17] In both cases, the barrier for chlorine diffusion is about 1 eV, and desorption takes place in the $SiCl_2$ form.[16,17] Furthermore, it was found that with increasing chlorine supply the structure of the chlorinated Si(111) surface suddenly changes, with a transition from a monochloride phase to a polychloride phase.[17] The adsorption of chlorine induces Cl-related Cl-Si bonding states below the top of the valence band.[15]

The reactive Si-Cl surface bonds are convenient for surface functionalization with alkene and amine groups.[23,24] Although Si-Cl bonds are stronger than Si-H bonds, the Cl atoms, with a higher affinity for electrons, can more easily receive an electron from the highest occupied molecular orbital (HOMO) of the other reactant during the interaction. This additional electron is partially localized on the shallowest p orbital of the Cl radical, resulting in Cl^- being released. Forming Cl^- in the transition state is energetically more favorable than breaking Si-H bonds, leading to lower activation energy barriers for grafting in Si-Cl bonds, even for partial Cl coverages.[24]

Additionally, the presence of chlorine changes the optical and electronic properties of the material, opening exciting possibilities for surface-driven electronic structure engineering. Previous electronic structure calculations have found that chlorine-covered nanocrystals have a lower gap between occupied and unoccupied electron energy levels and higher electron affinity than hydrogen-covered nanocrystals.[25,26] Thus it is possible that partial or full surface chlorination can be used to control the position of the electronic levels for specific applications.

Given the interest on Cl-terminated nanocrystals, both for subsequent surface conversion or for electronic structure engineering, theoretical information on the stability, electronic, and optical properties of silicon nanocrystals is of great interest. Therefore, we have carried out a detailed theoretical study to compare the properties of Cl-terminated silicon nanocrystals with 1–3 nm of diameter with H-terminated nanocrystals in the same size range. The first-principles methodology will be described in Sec. II. The structure and energetics of

pristine nanocrystals with Cl, H, and mixed terminations will be considered in Sec. III, and their electronic and optical properties will be given in Sec. IV. Section V is dedicated to doped and defective Cl- and H-terminated clusters. Finally, Sec. VI discusses the relevance of the results.

II. METHODOLOGY

The electronic structure of the nanocrystals was analyzed using first-principles calculations based on density functional theory, with a pseudopotential approach, as implemented in the AIMPRO code.[27,28] The local density approximation (LDA)[27] was used for the exchange and correlation energy. Core electrons were accounted for by using the pseudopotentials of Hartwigsen *et al*.[29]

Kohn-Sham orbitals were expanded on a localized basis set consisting of atom-centered Cartesian Gaussian orbitals with angular momentum up to $l = 2$, as described in Ref. 30. For the core silicon atoms, we used a contracted basis set with 13 functions per atom (44G*), including a polarization function with $l = 2$, optimized for bulk silicon. A basis of the same size, optimized for SiH_4, was used for hydrogen. For chlorine, an uncontracted basis set with four $l = 0$ and twelve $l = 1$ functions per atom was used. Convergence tests for silane, tetrachlorosilane, and $Si_{87}H_{76}/Si_{87}Cl_{76}$ nanocrystals show that these bases offer an excellent compromise between accuracy and computational effort, specially for large nanocrystal diameters, where the electronic structure becomes increasingly bulklike. For the worst case, the SiH_4 and $SiCl_4$ molecules, Si-H and Si-Cl bond lengths (Table I) are converged, respectively, within 0.006 and 0.015 Å, bond energies are converged within 0.1 and 0.5 eV, respectively, and the Kohn-Sham gaps are converged with 0.22 and 0.09 eV, respectively. They are also in good agreement with previous LDA calculations.

Total energy calculations were performed in real space. The optical absorption cross section was calculated using periodic boundary conditions, ensuring a minimum distance of at least 10 Å between replicas of the system. In this case, the charge density was expanded in a plane wave basis set with an energy cutoff of 350 Ry.

The equilibrium geometry of the nanocrystals was found by a relaxation of all the atomic coordinates using a conjugate gradient algorithm.

The optical absorption cross section was calculated in the long-wavelength dipole approximation using the Kohn-Sham eigenvalues E^n and eigenvectors $|\psi^k\rangle$. The matrix elements of $\mathbf{r}$ are evaluated using the momentum operator plus the commutator of the nonlocal part of the pseudopotential.[31] The Brillouin zone sampling was restricted to the Γ point. The electronic temperature used as parameter in the Fermi-Dirac distribution was 0.1 eV/k_B, where k_B is the Boltzmann constant, and the Gaussian broadening used was 0.05 eV.

III. STRUCTURE AND ENERGETICS

A. Structure

The nanocrystals used in this study were obtained by cutting an approximately spherical core out of a perfect silicon crystal and passivating the surface dangling bonds with Cl or H atoms. The cutoff diameter can be estimated as $d = [3n/(4\pi)]^{1/3}a_0$, where n is the number of silicon atoms and a_0 is the calculated lattice parameter of bulk silicon (5.39 Å). The surface silicon atoms were fourfold coordinated

TABLE I. Bond length, bond enthalpy, Kohn-Sham gap ($\Delta E_{KS} = E_{LUKS} - E_{HOKS}$), and vertical excitation energy of the SiH_4 and $SiCl_4$ molecules calculated with the method used in this work. Results from gradient and hybrid functional calculations[32] and from previous calculations are shown for comparison. PBE and HSE refer to the exchange-correlation functionals from Refs. 33 and 34, respectively.

Property		$l_{Si\text{-}X}$ (Å)	ΔH_b (eV)	ΔE_{KS}	ΔE^*
SiH_4	This work (LDA)	1.49	3.8	7.9	
	PBE[a]	1.51	3.2	7.7	
	HSE[a]	1.51	3.3	8.8	
	Prev. calc.	1.50[b]	3.5[c]	7.93[f]	8.76[f]
					9.26[g]
	Expt.	1.48[i]	3.3[d]		
			3.2[e]		
$SiCl_4$	This work (LDA)	2.03	4.3	6.1	6.5
	PBE[a]	2.09	3.8	5.4	
	HSE[a]	2.08	3.8	7.2	
	Prev. calc.				9.14[h]
	Expt.	2.02[i]	4.0[e]		

[a]Plane-wave calculation, see note.[32]
[b]All-electron LDA calculation from Ref. 37.
[c]All-electron LDA calculation from Ref. 38.
[d]From Ref. 39.
[e]From the heats of formation in Ref. 40.
[f]GGA-PBE calculation from Ref. 41.
[g]B3LYP calculation from Ref. 42.
[h]Discrete variational $X\alpha$ calculation.[43]
[i]From Ref. 44.

TABLE II. Atomic composition, diameter, and symmetry of the Si_nX_m nanocrystals studied, where $X \in \{H,Cl\}$.

n	m	d (nm)	Sym.
35	36	1.1	T_d
87	76	1.5	T_d
244	144	2.1	T_d
275	172	2.2	T_d
286	170	2.2	D_{3d}
377	196	2.4	T_d
513	252	2.7	T_d
717	300	3.0	T_d

and had mono- or dihydride/chloride termination. The number of Si and Cl or H atoms in each nanocrystal is given in Table II. All the nanocrystals were centered at an atomic site, with exception of the $Si_{286}X_{170}$ nanocrystals, which were centered at a bond center.

After atomic relaxation, all silicon atoms remain fourfold coordinated, and the lengths and angles of the Si-Si bonds are close to those of the bulk crystal, specially at a greater distance from the surface [Figs. 1(a), 1(d), and 1(g)]. Both Cl- and H-terminated nanocrystals maintain a marked crystalline character, characterized by a discrete radial pair distribution function relative to the nanocrystal center. However, there are quantitative differences between Cl- and H-covered nanocrystals. As highlighted in Fig. 1, the bond length distribution is much broader for the chlorinated nanocrystals. For example, for $d = 1.5$ nm, the average Si-Si bond length of the Cl- and H-terminated nanocrystals deviates only -0.01 and $+0.02$ Å, respectively, from the calculated bulk Si-Si bond length (2.34 Å), but the standard deviation is four times larger for the latter (Table III). The atomic radius of Cl is larger than that of H. Furthermore, Cl is more electronegative than H. Thus, the steric repulsion of the Cl surface atoms, which is longer ranged than for H atoms, leads to a distortion of the silicon lattice, specially close to the surface. For the smallest nanocrystals, this surface effect extends to the core layers of the nanocrystal. Since the effective radius of the Cl atom is closer to that of the silicon atom, in the chlorinated nanocrystal the bond angles are closer to the bulk value.

TABLE III. Average Si-Si, Si-Cl, and Si-H bond lengths ($\bar{l}_{X\text{-}Y}$) and angles ($\bar{\alpha}$), and their standard deviations, for a nanocrystal with diameter $d = 1.5$ nm, as a function of the surface Cl coverage ratio (x). Lengths are given in angstroms and angles in degrees. The experimental bulk Si-Si bond length is 2.35 Å.

x	0	0.25	0.5	0.75	1	Bulk Si
$\bar{l}_{\text{Si-Si}}$	2.33	2.33	2.33	2.34	2.36	2.34
$\bar{l}_{\text{Si-Cl}}$	–	2.10	2.09	2.09	2.07	
$\bar{l}_{\text{Si-H}}$	1.72	1.69	1.68	1.69	–	
$\Delta l_{\text{Si-Si}}$	0.0084	0.0095	0.014	0.024	0.04	
$\Delta l_{\text{Si-Cl}}$	–	0.012	0.044	0.072	0.0098	
$\Delta l_{\text{Si-H}}$	0.39	0.38	0.36	0.38	–	
$\bar{\alpha}$	103.2	106.0	108.2	109.3	109.4	109.5
$\Delta\alpha$	20.4	15.9	11.2	7.5	4.0	

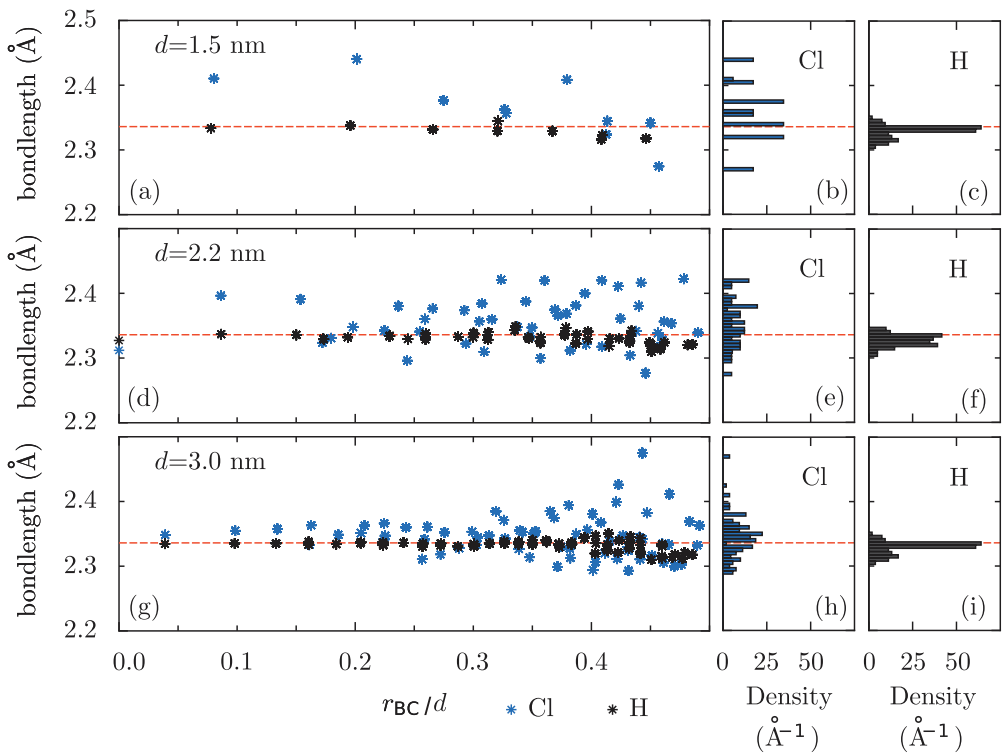

FIG. 1. (Color online) Calculated Si-Si bond lengths as a function of the distance of the bond center to the center of the nanocrystal (r_{BC}), and respective bond length histograms, for three nanocrystal diameters: (a)–(c) 1.5 nm, (d) and (e) 2.2 nm (D_{3d}), and (f)–(h) 3.0 nm. The dashed line represents the bulk Si bond length.

The Si-H surface bonds are elongated about 0.2 Å with respect to their length in the SiH_4 molecule (1.49 Å, to be compared with the experimental value 1.48 Å[44]). However, the Si-Cl bond lengths are very close to those of $SiCl_4$ (2.03 Å, to be compared with the experimental value of 2.02 Å[44]).

We now analyze the structure of nanocrystals with a mixed Cl/H surface. The fraction x of Cl atoms was varied between 0 and 1 ($x \in 0.25, 0.50, 0.75$), where x is the ratio between the number of Cl atoms and the total number of Cl and H atoms. For each x, the bond lengths and angles were averaged over 24 randomly generated samples (Table III). We notice that for the three intermediate x fractions the distribution of Si-Si bond lengths is more narrow than for $x = 1$ (Cl-covered nanocrystal), whereas the bond angle distribution is more narrow than for $x = 0$ (H-covered nanocrystal).

B. Formation and reaction enthalpies

It is important to know how the passivation with Cl affects the stability of the nanocrystals. Although highly metastable structures can be prepared out of equilibrium, for example, in nonthermal plasmas, the enthalpy of formation characterizes the stability in equilibrium and estimate reaction energies. It is therefore useful to evaluate the enthalpy of formation of the nanocrystals with Cl-covered surface or with mixed Cl and H surface passivation.

We calculated the formation enthalpies at $T = 0$, defined as the enthalpy change relative to the standard phases of Si (crystalline Si), Cl (molecular Cl_2), and H (molecular H_2):

$$H_f = E_{NC}(n, m_{Cl}, m_H) - nE_{Si} - \tfrac{1}{2}m_{Cl}E(Cl_2) - \tfrac{1}{2}m_H E(H_2), \quad (1)$$

where $E_{NC}(n, m_{Cl}, m_H)$ is the calculated total energy of $Si_nCl_{m_{Cl}}H_{m_H}$, and $E(Si)$, $E(Cl_2)$, and $E(H_2)$ are the total energy per atom of crystalline silicon and the total energies of the Cl_2 and H_2 molecules, respectively, calculated using the same approximations. A negative value of H_f means that the formation of the nanocrystal from the standard forms of the constituting elements is exoenthalpic.

We note that the total energies of small molecules, in particular H_2, are not accurately calculated using the LDA approximation. Thus our calculated formation enthalpies of $SiCl_4$ and SiH_4 are underestimated: We obtain −7.1 and −0.2 eV, respectively, whereas the experimental values are −6.6 and 0.4 eV.[40] However, this error often cancels out when calculating reaction energies. For example, the enthalpy change for the hydrogen replacement reaction

$$SiH_4 + Cl_2 \rightarrow SiH_3Cl + HCl, \quad (2)$$

which is −2.83 eV in our calculation, is only underestimated by 0.06 eV (relative to the value obtained from the experimental heats of formation[40]). Thus, the calculated formation enthalpies can still be used to draw qualitative conclusions.

Nanocrystal formation enthalpies are shown in Fig. 2(a). Cl-covered clusters have lower H_f than H-covered clusters, typically by 1.1–1.6 eV per surface Si-H or Si-Cl bond. This difference is larger than the difference between the bond energies in the $SiCl_4$ and SiH_4 molecules (Table I). It is also larger than the errors in $H_f(SiCl_4)$ and $H_f(SiH_4)$.

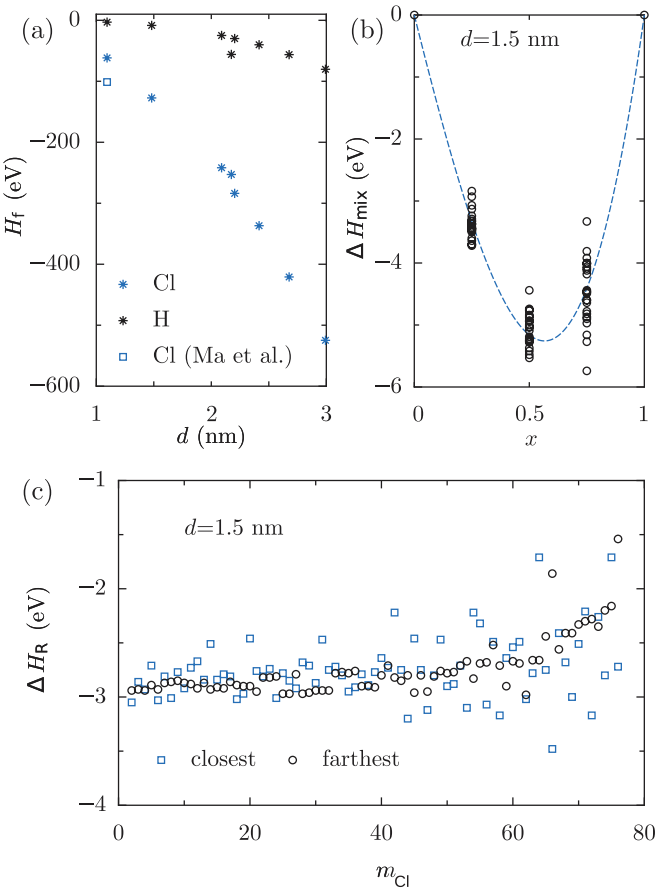

FIG. 2. (Color online) Stability of $Si_nCl_{m_{Cl}}H_{m_H}$ nanocrystals. (a) Enthalpy of formation of Cl- and H-terminated nanocrystals as a function of the diameter. (b) Mixing enthalpy [Eq. (3)] of $d = 1.5$ nm nanocrystals with mixed surface as a function of the Cl fraction $x = m_{Cl}/(m_{Cl} + m_H)$. (c) Comparison of the Cl replacement enthalpy [Eqs. (4) and (5)] for an even distribution of Cl (placement of each Cl in the farthest position from the existing $m_{Cl} - 1$ chlorine atoms) and for a concentrated distribution of Cl (placement of Cl in the nearest position to the existing $m_{Cl} - 1$ chlorine atoms) for $d = 1.5$ nm.

The enthalpy of formation of the clusters with mixed Cl/H surface follows very closely a linear interpolation of the endpoints $x = 0$ and $x = 1$. In analogy with the alloys, we can define a mixing enthalpy characterizing the deviation from linearity:

$$\Delta H_{mix} = E_{NC}(n, m_{Cl}, m_H) - [E_{NC}(n, m_{Cl} + m_H, 0) - E_{NC}(n, 0, m_{Cl} + m_H)]. \quad (3)$$

This is given in Fig. 2(b) for $d = 1.5$ nm. The mixing enthalpy ΔH_{mix} is negative and smaller by one or two orders of magnitude than the enthalpy of formation. If, near the temperature at which the Cl and H atoms become mobile, the mixing free energy remains negative, this means that a binary system with Si_nCl_m and Si_nH_m moieties will be unstable against the formation of a mixed $Si_nCl_{m_{Cl}}H_{m_H}$ ensemble.

Since the effective radius of the Cl atoms is much larger than that of H atoms, an additional question is whether steric effects prevent Cl atoms from occupying neighboring positions, even preventing complete chlorination altogether. To investigate this we calculated the enthalpy change associated with the

hydrogen replacement reactions,

$$Si_nCl_{m_{Cl}-1}H_{m_H+1} + Cl_2 \rightarrow Si_nCl_{m_{Cl}}H_{m_H} + HCl \quad (4)$$

for $m_{Cl} < n$, which is given by

$$\Delta H_R = E_{NC}(n,m_{Cl},m_H) + E(HCl) - [E_{NC}(n,m_{Cl}-1,m_H+1) - E(Cl_2)] \quad (5)$$

for $d = 1.5$ nm nanocrystals. Two situations were considered. Starting with $Si_{87}ClH_{75}$, we first created an even distribution of Cl by placing each additional Cl atom in one of the surface sites (position $\mathbf{r}$) minimizing the function

$$f(\mathbf{r}) = \sum_{i=1}^{m_{Cl}-1} |\mathbf{r} - \mathbf{r}_i|^{-1}. \quad (6)$$

This results in a sequence of clusters where Cl replacing for H takes place at the position further away from all the other Cl atoms. The enthalpy changes for this sequence of replacements are compared with those obtained for a concentrated Cl distribution, where each Cl atom is placed as close as possible to the atoms of the same species [thus maximizing $f(\mathbf{r})$]. The results [Fig. 2(c)] show that there is no clear energetic preference for the first process, although the distribution of the enthalpies of replacement is smoother and narrower. Moreover, the enthalpies of replacement stay approximately constant up to 50% coverage, showing only a slight increase for higher x. So, there is in principle no reason why complete Cl coverage would not be attainable.

IV. ELECTRONIC AND OPTICAL PROPERTIES

A. Analysis of the Kohn-Sham states

Let us start by analyzing the electronic structure of the $SiCl_4$ and SiH_4 molecules, as represented by the Kohn-Sham eigenstates and eigenvalues. Although these quantities have only an auxiliary role in DFT, their analysis is useful to understand the bonding and the contribution of Cl and H atoms to the ground state and excited states. The highest occupied state of the $SiCl_4$ molecule is the $2t_1$ state, followed closely by the $2e$ and $8t_2$ states. The highest occupied Kohn-Sham state (HOKS) is completely localized on the Cl atoms (formed by Cl $3p$ states). The $2e$ and $8t_2$ states also have a localization of less than 10% on the Si atom. In contrast, the HOKS of SiH_4, which is the $2t_2$ state, is a bonding state 41% localized in the Si atom. The lowest unoccupied state of the $SiCl_4$ molecule is the $8a_1$ state, followed 1.7 eV above by the $9t_2$ state, whereas the lowest unoccupied Kohn-Sham state (LUKS) of SiH_4 is $3t_2$. Both are partially localized on Si: 54% in the case of the $SiCl_4$ LUKS and 65% in the case of the SiH_4 LUKS.

As the number of Si atoms increases, the HOKS state and the LUKS start to resemble the bulk silicon valence and conduction band states, but in the case of the Cl-covered clusters the Cl $3p$ character is maintained. Figure 3 depicts the charge density associated with the HOKS (triplet) and LUKS states for $d = 1.5$ nm. The localization of those gap-edge states on the surface atoms is greater for the Cl-covered cluster, specially for the HOKS state (the fractional HOKS localizations on Cl/H are, respectively, 40% and 9% for the Cl- and H-covered NCs). The contribution of the Cl $3p$ atomic orbitals to the HOKS state is evident in the shape of the charge density isosurface near the surface of the nanocrystal, which resembles the $SiCl_4$ $2t_1$ state. Similarly, near the surface the LUKS state bears some resemblance to the $SiCl_4$ LUKS ($8a_1$) state.

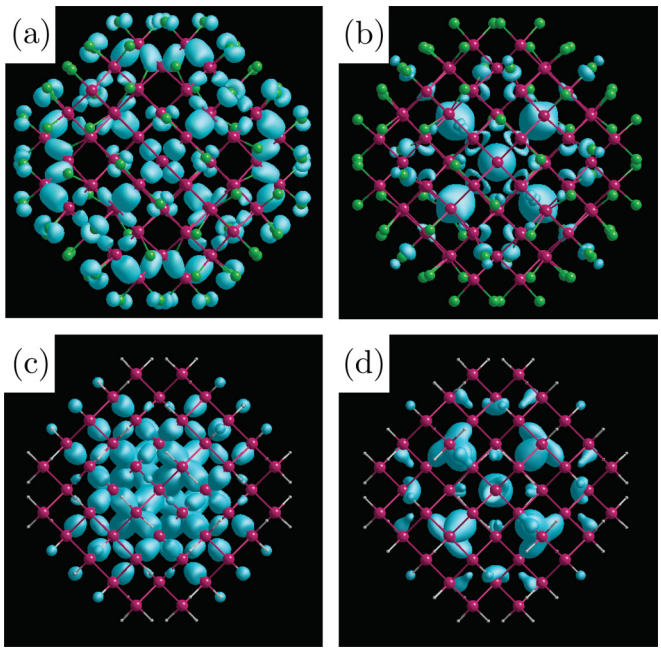

FIG. 3. (Color online) Charge density associated with the HOKS and LUKS levels: (a) HOKS of Cl-covered nanocrystal, (b) LUKS of Cl-covered nanocrystal, (c) HOKS of H-covered nanocrystal, and (d) LUKS of H-covered nanocrystal. The isosurface value is 3×10^{-3} and 8×10^{-4} for HOKS and LUKS states, respectively.

The calculated HOKS-LUKS gap (E_{KS}) of the SiH_4 and $SiCl_4$ molecules is, respectively, 7.93 and 6.96 eV (Table I). Although these are not far from the experimental absorption energy thresholds, which are, respectively, 8.99[45] and 8.84 eV,[46] there are several reasons why they cannot be compared directly to experiment. First, the HOKS and LUKS states of $SiCl_4$ are $2t_1$ and $8a_1$, respectively, and the HOKS→LUKS optical transition is forbidden by symmetry; the lowest allowed transition $2t_1 \rightarrow 9t_2$ corresponds to an eigenvalue energy difference of 8.1 eV. Moreover, the Kohn-Sham states change considerably in the excited state, and so do Coulomb, exchange, and correlation interactions. Moreover, the threshold energy of the absorption spectra of both molecules is a Rydberg transition ($4s \rightarrow 8t_2$).[45,46] These excitonic effects leading to Rydberg states are not described by the ground state DFT. To our knowledge, Rydberg transitions have not been resolved for undoped silicon nanocrystals.

For silicon nanocrystals with diameters between 1 and 3 nm, the lowest excitation energy, obtained by calculating the difference between the total energies of each nanocrystal in the ground state and in the first excited state (at the ground state geometry), $E^x_{LDA} = E^1_G - E^0_G$, differs little from E_{KS} (Fig. 4). This means that upon excitation the change in the electrostatic interaction energy (resulting from the interaction between electron, hole, and image charges) is partially canceled by the change in the exchange and correlation energy.

The excitation energy (E_x) of hydrogenated nanocrystals has been previously calculated at different levels of theory (see, for example, Refs. 41 and 47–49). As illustrated in Fig. 4,

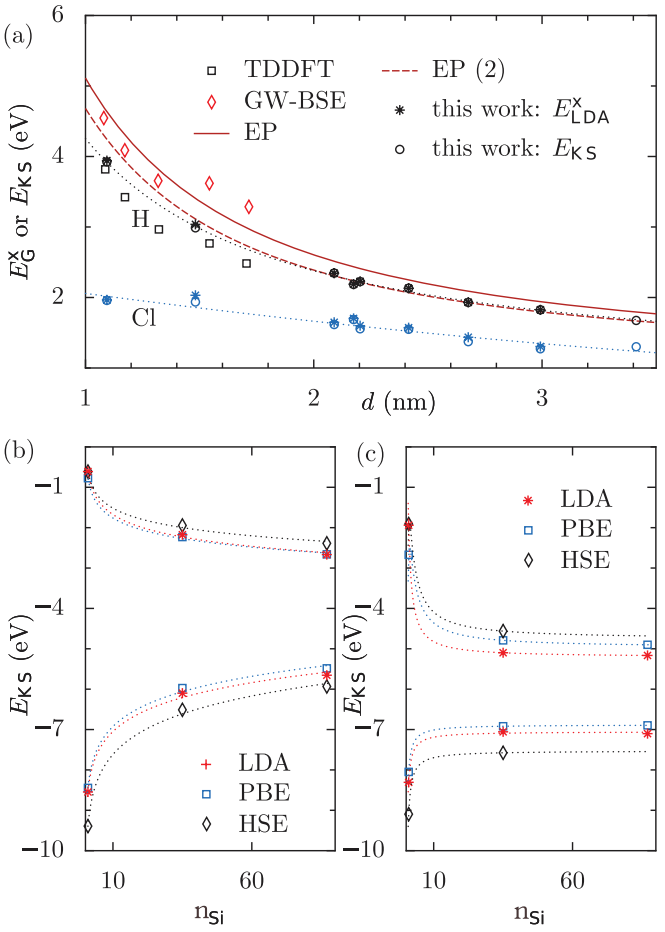

FIG. 4. (Color online) (a) Excitation energy (*) and Kohn-Sham band gap (○) as a function of the nanocrystal diameter obtained from the present work. Data from previous calculations are shown for comparison: Lowest excitation energy excitations calculated by solving the Bethe-Salpeter equation (GW-BSE) from Ref. 48, or obtained by time-dependent LDA (TDLDA), also from Ref. 48, calculated using empirical pseudopotentials without inclusion of the Coulomb interaction between electron and hole (EP) or including this contribution (EP2), from Ref. 47. (b) Comparison of the LUKS and HOKS energies for H-terminated nanocrystals, calculated using the approximations employed in this work (LDA), or using gradient or hybrid functional approaches.[32] (c) Comparison of the LUKS and HOKS energies for Cl-terminated nanocrystals. Dotted lines are a guide to the eye.

our results are in good agreement with previous calculations with empirical potentials, and differ less than 1 eV from GW gaps. The reason why the LDA HOKS-LUKS band gap is a good approximation for the excitation energy is clarified by Delerue *et al.*, who have proved that the differences between the corrections to the self-energy in bulk and in the nanocrystal ($\delta\Sigma E$) are nearly canceled out by the Coulomb interaction between electron and hole (E_C). As a result, $E_x \simeq E_{KS} + \delta\Sigma_b$, where $\delta\Sigma_b$ is the bulk self-energy correction, which is about 0.6–0.7 eV for the LDA approximation. In this work we will assume that this correction is independent of the nanocrystal surface, thus justifying the comparison between Cl- and H-covered nanocrystals using the values directly obtained from first principles.

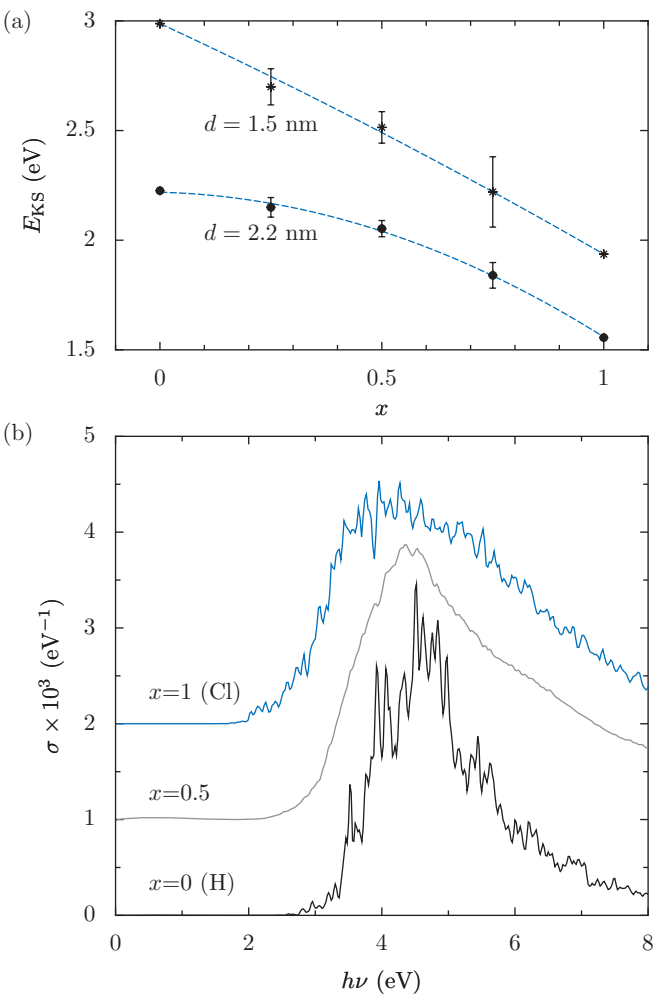

FIG. 5. (Color online) Kohn-Sham band gap (a) and calculated absorption spectra (b) of $d = 2.2$ nm silicon nanocrystals for different fractions of Cl coverage [$x = m_{Cl}/(m_{Cl} + m_H)$]. The eigenvalue gaps for fractional x were obtained by averaging over 24 samples, and the error bars represent the standard deviation of the results. The absorption spectra for $x = 0.5$ was obtained by averaging over ten samples.

The minimum excitation energy is lower for the Cl-covered nanocrystal than for the H-covered nanocrystal. This follows the lower effective confinement volume for the HOKS and LUKS states in the Cl-covered nanocrystals. The difference is greater for the smaller diameters, amounting to about 1 eV for $d \sim 1.5$ nm. With increasing d, the gap of the Cl-covered clusters decreases almost linearly in this size range, whereas that of the H-covered nanocrystals varies approximately with $d^{-1.2}$. The average gap of nanocrystals with mixed Cl and H coverage varies monotonically between those of the Cl- and H-covered clusters of the same size (Fig. 5). The variation in the gap distribution for each set of samples with the same d and x is not negligible, and is represented in Fig. 5 by the error bars.

B. Optical spectra

We have calculated the optical absorption cross section directly using the Kohn-Sham eigenstates and eigenvalues,

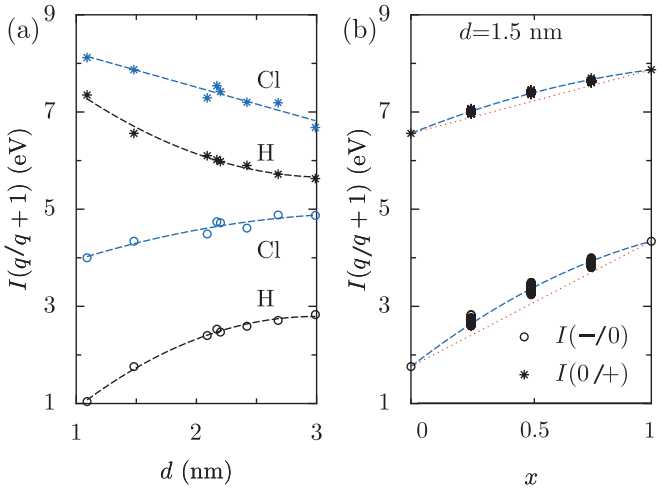

FIG. 6. (Color online) Ionization energy $[I(0/+)]$ and electron affinity $[I(-/0)]$ (a) for Cl- and H-covered nanocrystals, as a function of the diameter, and (b) for $d = 1.5$ nm nanocrystals with mixed surface ($Si_{87}Cl_{m_{Cl}}H_{m_H}$), as a function of the Cl fraction $x = m_{Cl}/(m_{Cl} + m_H)$.

as described in Sec. II. Previous theoretical work has shown that optical spectra can, in a good approximation, be obtained from the Kohn-Sham eigenvalues since only minor charge rearrangements occur between ground and the low excited states.[50] As expected, the absorption threshold energy is lower for the Cl-covered cluster (Fig. 5). However, the energies close to E_{KS} have very small or vanishing oscillator strengths. The threshold is steeper for the H-covered nanocrystal and for the nanocrystal with mixed surface, where the symmetry is broken, than for the Cl-covered nanocrystals. Overall, the absorption band in the 2–6 eV range is broader for the Cl-covered nanocrystal.

C. Ionization energy and electron affinity

The ionization energy was obtained from the total energies of neutral and charged clusters,

$$I(q/q+1) = E(q+1) - E(q), \tag{7}$$

where q is the charge. The results are shown in Fig. 6. The electron affinity of the chlorinated nanocrystals is higher by 2–3 eV for the whole range of d considered, reflecting the higher affinity for electrons of Cl. The ionization energy is also higher, but only by about 1 eV.

V. DEFECTS

A. Dopants

Furthermore, we compare the ionization energy/electron affinity of doped nanocrystals with that of the pristine (undoped) nanocrystals. This comparison is relevant when doping nanocrystal composites where only a small fraction of nanocrystals encloses one or more dopant atoms. In that case, the ideal is that a nanocrystal doped with a shallow donor (for example P) has ionization energy $I(0/+)$ very close to the electron affinity $I(-/0)$ of the undoped nanocrystal. Ideally, $I_P(0/+) - I_{UD}(-/0)$, where the subscripts label the doped and undoped nanocrystals and should be comparable

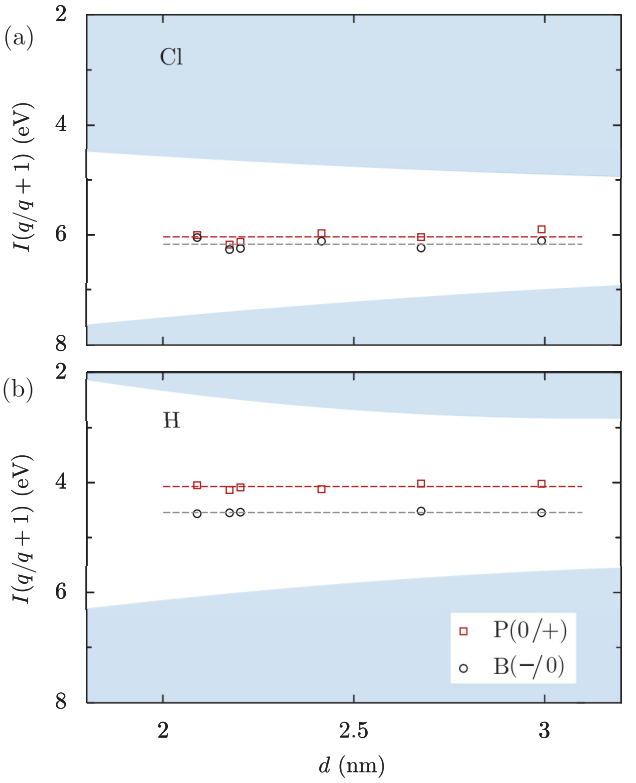

FIG. 7. (Color online) Ionization energy $[I(0/+)]$ and electron affinity $[I(-/0)]$ of doped and undoped (a) Cl-covered nanocrystals and (b) H-covered nanocrystals, as a function of the diameter. Shaded areas represent energies lower than the electron affinity or higher than the ionization energy of the undoped nanocrystal. The axis were inverted for easier visualization.

to kT, where T is the temperature and k is the Boltzmann constant. The reverse is true for shallow acceptors. However, this does not happen either for Cl- or H-covered nanocrystals with d between 2 and 3 nm (Fig. 7). This is due to the carrier confinement and appearance of image charges, which were already extensively discussed for H-covered nanocrystals.[51–55]

B. Dangling bonds

The position of the donor and acceptor levels of surface dangling bonds (DBs) relative to the gap-edge states of the pristine nanocrystals has also been compared for both types of surface. We considered only dangling bonds on dichloride or dihydride surface silicon atoms, that is, those that in the pristine nanocrystal were attached to two surface terminators. In $d = 1.5$ nm nanocrystals, monohydride DBs, although on average higher in energy by 0.9 eV, have similar properties. For each NC size there are several nonequivalent surface Si atoms with dichloride (or dihydride) terminations where dangling bonds can form. The geometry and energy of each of the respective defects was optimized independently.

First, we note that the $(-/0)$ and $(0/+)$ level positions do not display a clear trend with the nanocrystal size. The DB levels are very dependent on the particular defect geometry, specially on the Cl-covered nanocrystals (Fig. 8). The main difference between Cl- and H-covered nanocrystals is that,

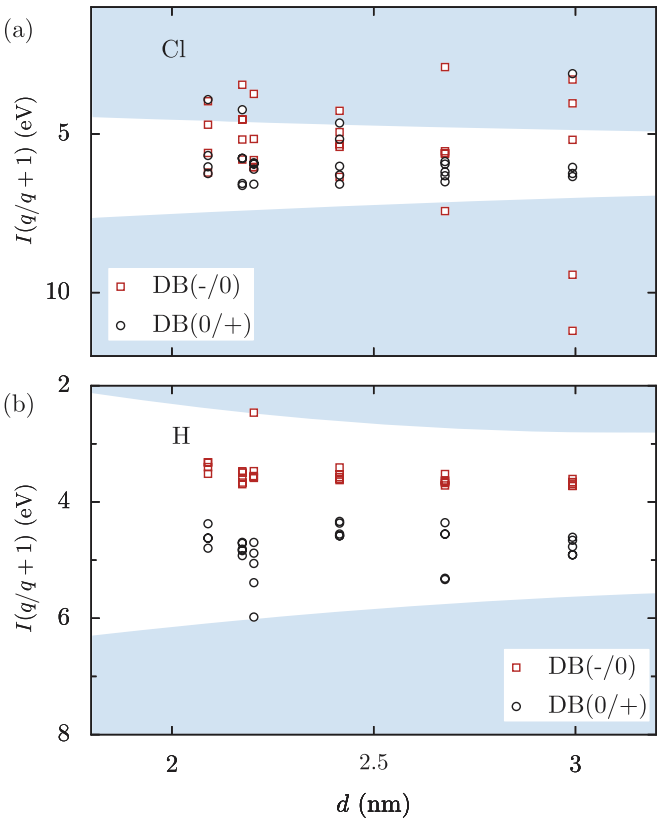

FIG. 8. (Color online) Incomplete ionization energy [$I(0/+)$] and electron affinity [$I(-/0)$] of surface dangling bonds on (a) Cl-covered nanocrystals and (b) H-covered nanocrystals, as a function of the diameter. Dangling bonds were formed on all symmetry-nonequivalent dihydride terminations. Shaded areas represent energies lower than the electron affinity or higher than the ionization energy of the undoped nanocrystal. The axis were inverted for easier visualization.

as the gap of the former is smaller, some of the DB levels fall outside the gap. That does not happen for the H-covered nanocrystals.

VI. DISCUSSION

Silicon NCs with chlorinated or mixed surface have two main potential uses: as an intermediate material for further surface functionalization and modification, and as an electronic or optoelectronic material. The energies and electronic properties obtained using local density functional theory may be useful to design or tune both types of applications.

We have show that the formation enthalpy of the chlorinated Si-NCs is more negative than that of the hydrogenated Si-NCs, relative to the standard states of Cl and H. However, this does not mean that the former will in general be more stable against reaction. In fact, chlorinated Si-NCs have very high electron affinity, and can easily trap electrons to the lowest occupied state, which is partially localized on the surface Cl orbitals (Fig. 3). This leaves Cl more susceptible to removal and substitution by a foreign radical. It is interesting to note that although mixed Cl and H surfaces have a negative mixing enthalpy, there is no strong repulsion between nearest-neighbor Cl atoms, specially for small coverage ratios. Thus, if the nanocrystals are kept neutral, there is in principle the possibility of engineering next-neighbor surface replacements using hydrogenated NCs with selected Cl substitutions.

Chlorine can be used to modify intentionally the electronic and optical properties of the Si-NCs. Chlorinated Si-NCs also have a smaller gap between occupied and unoccupied electron levels. As a result, the threshold energy for optical absorption is redshifted. The absorption edge can be varied by changing the Cl coverage ratio.

As both the electron affinity and ionization energy are greater than those of hydrogenated silicon nanocrystals, the Cl surface coverage ratio can be used to tune the alignment between the Si-NC states and the bands of other materials in heterojunctions. Chlorinated Si-NCs doped with P (or B) have ionization energy (electron affinity) levels quite distant from the $(-/0)$ $[(0/+)]$ levels of pristine nanocrystals with the same size. This also happens with hydrogenated Si-NCs, and makes it difficult for a doped NC to donate free carriers to undoped nanocrystals. However, as the gap of the chlorinated Si-NCs shifted to lower energies, P$(0/+)$ and B$(-/0)$ levels are also shifted relative to the vacuum level, in comparison with the hydrogenated crystals. This knowledge may be useful to design heterojunctions with doped Cl-terminated Si-NCs as one of the components. As in the hydrogenated Si-NCs, dangling bonds will act as exciton recombination centers.

ACKNOWLEDGMENTS

The computations were performed on resources provided by the Swedish National Infrastructure for Computing (SNIC) at KTH (Lindgren), Umeå University (Akka), University of Aveiro (Blafis), and University of Coimbra (Milipeia). This work was supported by the Calouste Gulbenkian Foundation, the Marie Curie Program REG/REA.P1(2010)D/22847 (SiNanoTune), and FCT Portugal.

*aicarvalho@ua.pt

[1] J. L. Heinrich, C. L. Curtis, G. M. Credo, M. J. Sailor, and K. L. Kavanagh, Science **255**, 66 (1992).
[2] R. A. Bley and S. M. Kauzlarich, J. Am. Chem. Soc **118**, 12461 (1996).
[3] L. Mangolini and U. Kortshagen, in *Silicon Nanocrystals; Fundamentals, Synthesis, and Applications*, edited by L. Pavesi and R. Turan (Wiley, Weinheim, 2010).
[4] L. Mangolini and U. Kortshagen, Adv. Mater. **19**, 2513 (2007).
[5] S. Oda, Adv. Colloid Interface Sci. **71–72**, 31 (1997).
[6] T. Ifuku, M. Otobe, A. Itoh, and S. Oda, Jpn. J. Appl. Phys. **36**, 4031 (1997).
[7] T. Nozaki, K. Sasaki, T. Ogino, D. Asahi, and K. Okazaki, Nanotechnology **18**, 235603 (2007).
[8] R. Gresback, T. Nozaki, and K. Okazaki, Nanotechnology **22**, 305605 (2011).

[9]X. Li, Y. He, Suddha S. Talukdar, and M. T. Swihart, Langmuir **19**, 8490 (2003).
[10]Y. Nakamine, N. Inaba, T. Kodera, K. Uchida, R. N. Pereira, A. R. Stegner, M. S. Brandt, M. Stutzman, and S. Oda, Jpn. J. Appl. Phys. **50**, 025002 (2011).
[11]A. R. Stegner, R. N. Pereira, R. Lechner, K. Klein, H. Wiggers, M. Stutzmann, and M. S. Brandt, Phys. Rev. B **80**, 165326 (2009).
[12]R. Lechner, A. R. Stegner, R. N. Pereira, R. Dietmueller, M. S. Brandt, A. Ebbers, M. Trocha, H. Wiggers, and M. Stutzmann, J. Appl. Phys. **104**, 053701 (2008).
[13]X. D. Pi, R. Gresback, R. W. Liptak, S. A. Campbell, and U. Kortshagen, Appl. Phys. Lett. **92**, 123102 (2008).
[14]J. M. Buriak, Chem. Rev. **102**, 1271 (2002).
[15]R. D. Schnell, D. Rieger, A. Bogen, F. J. Himpsel, K. Wandelt, and W. Steinmann, Phys. Rev. B **32**, 8057 (1985).
[16]G. A. de Wijs, A. De Vita, and A. Selloni, Phys. Rev. Lett. **78**, 4877 (1997).
[17]S. Sakurai and T. Nakayama, Surf. Sci. **493**, 143 (2001).
[18]S. Sakurai and T. Nakayama, J. Cryst. Growth **237–239**, 21 (2002).
[19]D. Humbird and D. B. Graves, J. Appl. Phys. **96**, 791 (2004).
[20]S. Rivillon, Y. J. Chabal, L. J. Webb, D. J. Michalak, N. S. Lewis, M. D. Halls, and K. Raghavachari, J. Vac. Sci. Tech. A **23**, 1100 (2005).
[21]S. D. Solares, H. Yu, L. J. Webb, N. S. Lewis, J. R. Heath, and W. A. Goddard, III, J. Am. Chem. Soc. **128**, 3850 (2006).
[22]S. M. Mohapatra, B. N. Dev, K. C. Mishra, N. Sahoo, W. M. Gibson, and T. P. Das, Phys. Rev. B **38**, 12556 (1988).
[23]J. Veinot, in *Silicon Nanocrystals; Fundamentals, Synthesis, and Applications*, edited by L. Pavesi and R. Turan (Wiley, Weinheim, 2010).
[24]F. A. Soria, E. M. Patrito, and P. Paredes, Langmuir **17**, 2613 (2011).
[25]A. Martínez, J. C. Alonso, and L. E. Sansores, J. Phys. Chem. C **114**, 12427 (2010).
[26]Y. Ma, X. Chen, X. Pi, and D. Yang, J. Phys. Chem. C **115**, 12822 (2011).
[27]P. R. Briddon and R. Jones, Phys. Status Solidi B **217**, 131 (2000).
[28]M. J. Rayson and P. R. Briddon, Comp. Phys. Commun. **178**, 128 (2008).
[29]C. Hartwigsen, S. Goedecker, and J. Hutter, Phys. Rev. B **58**, 3641 (1998).
[30]J. P. Goss, M. J. Shaw, and P. R. Briddon, in *Theory of Defects in Semiconductors*, edited by D. A. Drabold and S. K. Estreicher, Topics in Applied Physics, Vol. 104 (Springer, Berlin, 2007), p. 6994.
[31]A. J. Read and R. J. Needs, Phys. Rev. B **44**, 13071 (1991).
[32]Calculations with the PBE[33] and HSE[34] hybrid functionals were performed using the plane-wave code CPMD,[35] with Troullier-Martins pseudopotentials,[36] and a 75 Ry energy cutoff.
[33]J. P. Perdew, K. Burke, and M. Ernzerhof, Phys. Rev. Lett. **77**, 3865 (1996).
[34]J. Heyd, G. E. Scuseria, and M. Ernzerhof, J. Chem. Phys. **118**, 8207 (2003); **124**, 219906 (2006).
[35]Cpmd v3.15.1, copyright IBM Corp. 1990–2006 and copyright MPI Stuttgart (1997–2008).
[36]N. Troullier and J. L. Martins, Phys. Rev. B **43**, 1993 (1991).
[37]R. O. Jones, B. W. Clare, and P. J. Jennings, Phys. Rev. B **64**, 125203 (2001).
[38]M. Ernzerhof and G. E. Scuseria, J. Chem. Phys. **110**, 5029 (1999).
[39]D. Feller and D. A. Dixon, J. Phys. Chem. A **103**, 6413 (1999).
[40]M. W. Chase Jr., C. A. Davies, J. R. Downey Jr., D. J. Frurip, R. A. McDonald, and A. N. Syverud, *NIST-JANAF Thermochemical Tables 1985*, Version 1.0, *NIST Standard Reference Database 13* (National Institute of Standards and Technology, Gaithersburg, MD, 1986).
[41]E. Degoli, G. Cantele, E. Luppi, R. Magri, D. Ninno, O. Bisi, and S. Ossicini, Phys. Rev. B **69**, 155411 (2004).
[42]O. Lehtonen and D. Sundholm, Phys. Rev. B **72**, 085424 (2005).
[43]H. Ishikawa, K. Fujima, and H. Adachi, J. Chem. Phys. **94**, 6740 (1991).
[44]R. D. Johnson III, ed., *NIST Computational Chemistry Comparison and Benchmark Database*, NIST Standard Reference Database Number 101 Release 15b, August 2011 [http://cccbdb.nist.gov/].
[45]M. Suto and L. C. Lee, J. Chem. Phys. **84**, 1160 (1986).
[46]T. Ibuki, M. Kono, Y. Asari, A. Hiraya, and K. Shobatake, J. Chem. Phys. **106**, 4853 (1997).
[47]J. P. Proot, C. Delerue, and G. Allan, Appl. Phys. Lett. **61**, 1948 (1992).
[48]M. L. Tiago and J. R. Chelikowsky, Phys. Rev. B **73**, 205334 (2006).
[49]X. Yang, Y.-J. Zhao, H. Xu, and B. I. Yakobson, Phys. Rev. B **83**, 205314 (2011).
[50]B. Delley and E. F. Steigmeier, Phys. Rev. B **47**, 1397 (1993).
[51]M. Lannoo, C. Delerue, and G. Allan, Phys. Rev. Lett. **74**, 3415 (1995).
[52]Z. Zhou, M. L. Steigerwald, R. A. Friesner, L. Brus, and M. S. Hybertsen, Phys. Rev. B **71**, 245308 (2005).
[53]D. V. Melnikov and J. R. Chelikowsky, Phys. Rev. Lett. **92**, 046802 (2004).
[54]T. L. Chan, M. L. Tiago, E. Kaxiras, and J. R. Chelikowsky, Nano Lett. **8**, 596 (2008).
[55]G. Cantele, E. Degoli, E. Luppi, R. Magri, D. Ninno, G. Iadonisi, and S. Ossicini, Phys. Rev. B **72**, 113303 (2005).